



ELSEVIER

Contents lists available at ScienceDirect

Fuel

journal homepage: www.elsevier.com/locate/fuel

Estimation and modeling of coal pore accessibility using small angle neutron scattering



Rui Zhang^a, Shimin Liu^{a,*}, Jitendra Bahadur^b, Derek Elsworth^a, Yuri Melnichenko^b, Lilin He^b, Yi Wang^a

^a Department of Energy and Mineral Engineering, G³ Center and Energy Institute, The Pennsylvania State University, University Park, PA 16802, USA

^b Biology and Soft Matter Division, Neutron Sciences Directorate, Oak Ridge National Laboratory, Oak Ridge, TN 37831, USA

HIGHLIGHTS

- Apply small-angle neutron scattering (SANS) to quantify pore accessibility in coal matrix.
- Propose and validate a pore accessibility model using SANS results.
- Estimate pore accessibility for two different rank coals.
- Pore accessibility and pore radius has a power-law relationship.

ARTICLE INFO

Article history:

Received 23 May 2015

Received in revised form 25 August 2015

Accepted 26 August 2015

Available online 4 September 2015

Keywords:

Pore accessibility

SANS

Coal pore characterization

Accessibility modeling

ABSTRACT

Gas diffusion in coal is controlled by nano-structure of the pores. The interconnectivity of pores not only determines the dynamics of gas transport in the coal matrix but also influences the mechanical strength. In this study, small angle neutron scattering (SANS) was employed to quantify pore accessibility for two coal samples, one of sub-bituminous rank and the other of anthracite rank. A theoretical pore accessibility model was proposed based on scattering intensities under both vacuum and zero average contrast (ZAC) conditions. The results show that scattering intensity decreases with increasing gas pressure using deuterated methane (CD₄) at low Q values for both coals. Pores smaller than 40 nm in radius are less accessible for anthracite than sub-bituminous coal. On the contrary, when the pore radius is larger than 40 nm, the pore accessibility of anthracite becomes larger than that of sub-bituminous coal. Only 20% of pores are accessible to CD₄ for anthracite and 37% for sub-bituminous coal, where the pore radius is 16 nm. For these two coals, pore accessibility and pore radius follows a power-law relationship.

© 2015 Elsevier Ltd. All rights reserved.

1. Introduction

Natural gas has a relatively lower CO₂-to-energy content than coal and oil and therefore has some advantages as a substitute fuel to reduce the carbon intensity of energy production. For this reason, as well as their newfound abundance, unconventional natural gas resources are progressively displacing coal and oil in static combustion [1]. Among all the unconventional gas reservoirs, coalbed methane (CBM) is one of the most important resources with a relatively low risk of development and its utilization has grown rapidly in the last few decades. Coal permeability and gas content are two of the most important parameters in the successful recovery of CBM and both are closely related to coal pore structure [2–4].

As an organic-rich material, coal has a complex pore architecture which is not fully understood [5]. The pore structure of coal

is heterogeneous and anisotropic and includes macropores (>50 nm), mesopores (2–50 nm), and micropores (<2 nm) [6]. Microporosity dominates in high rank coals, while most of the porosity present in low rank coals is distributed in the macropore range [7]. Within the same rank, high-vitrinite bituminous coals have more micropores than low-vitrinite bituminous coals, which affect gas adsorption capacity [8]. The connectivity of micropores exerts a significant contribution to gas diffusion in micropores and to overall permeability [9]. The fraction of accessible pores becomes increasingly important in various areas, such as, the estimation of original gas-in-place (GIP), and in the prediction of gas production, permeability evolution, recovery of enhanced coalbed methane (ECBM) and in estimate of mass of carbon potentially sequestered [10].

Many techniques have been applied to investigate pore accessibility in porous media – each method with advantages and limitations. Optical microscopy, scanning electron microscopy (SEM) and transmission electron microscopy (TEM) can only give qualitative

* Corresponding author. Tel.: +1 8148634491; fax: +1 8148653248.

E-mail address: szl3@psu.edu (S. Liu).

Nomenclature

Q	scattering vector or momentum transfer	b	difference of power law exponent between vacuum and zero average contrast conditions
λ	neutron wavelength	R	pore radius
θ	scattering angle	a'	equals to $a \times (0.25)^b$
$I(Q)$	scattering intensity at a certain scattering vector	b'	equals to $-b$
\varnothing	volume fraction of a phase		
$\gamma_0(r)$	correlation function		
ρ_s^*	scattering length density of solid matrix		
ρ_f^*	scattering length density of fluid in pores		
N_A	Avogadro's constant		
d	bulk density (solid matrix or fluid in the pores)		
M	pseudo-molar mass of a phase		
p_j	proportion of compound j in a mixture		
s_i	proportion of nucleus i in compound j		
b_i	coherent scattering amplitude of nucleus i		
$I(Q, ZAC)$	scattering intensity at zero average contrast condition		
$I(Q, VAC)$	scattering intensity at vacuum condition		
$C_{AC}(Q)$	fraction of accessible pores (pore accessibility)		
C_p	power law constant (contrast factor)		
α	power law exponent		
B	incoherent background		
$I_{subtracted}(Q)$	background-subtracted scattering intensity		
$I_{subtracted, VAC}(Q)$	background-subtracted scattering intensity at vacuum condition		
$I_{subtracted, ZAC}(Q)$	background-subtracted scattering intensity at zero average contrast condition		
$C_{p, VAC}$	contrast factor at vacuum condition		
$C_{p, ZAC}$	contrast factor at zero average contrast condition		
α_{VAC}	power law exponent at vacuum condition		
α_{ZAC}	power law exponent at zero average contrast condition		
a	ratio of contrast factor between zero average contrast and vacuum conditions		

Abbreviations

SANS	small angle neutron scattering
ZAC	zero average contrast
CBM	coalbed methane
GIP	gas-in-place
ECBM	enhanced coalbed methane
SEM	scanning electron microscopy
TEM	transmission electron microscopy
Micro-XCT	micro X-ray computed tomography
MIP	mercury intrusion porosimetry
LPGA	low-pressure gas (N ₂ /CO ₂) adsorption
PSD	pore size distribution
SSA	specific surface area
1D	one dimensional
2D	two dimensional
SLD	scattering length density
SAXS	small angle X-ray scattering
ORNL	Oak Ridge National Laboratory
GP-SANS	general-purpose small angle neutron scattering diffractometer
XRD	X-ray diffraction
EOS	equation of state

information within a very limited window of observation [11]. Micro X-ray computed tomography (Micro-XCT) cannot provide details at nano-scale resolution required for characterization [12]. Mercury intrusion porosimetry (MIP) and low-pressure gas (N₂/CO₂) adsorption (LPGA) are invasive methods, which can only detect the accessible pore structures but also may destroy the samples [8]. Fortunately, small angle neutron scattering (SANS), as an emerging technique for investigating pore structure in porous media, has recently been applied in quantitatively characterizing pore accessibility in geomaterials [10,13–20]. Historically, SANS has been employed in the micropore characterization of coal [21,22], but has recently been applied to quantify coal pore accessibility [10,13,14].

MIP, LPGA and SANS techniques have been used to obtain the pore size distribution (PSD) of six coals of varying rank [23]. The porosity estimated from SANS data is larger than that of both MIP and LPGA for all six samples. This is because SANS detects both open and closed pores while MIP and LPGA only probe open pores [23]. Similarly, specific surface area (SSA) estimated by SANS is larger than that obtained by LPGA technique for both coal and shale samples, which is also due to capability of SANS in detecting both open and closed pores [24].

A new methodology was recently developed for determining pores accessible to deuterated methane (CD₄) and CO₂ for three coals and one porous silica [10], which found that pore accessibility in coals may have a positive correlation with total porosity and that pore accessibility may not only depend on pore size but also on fluid type, temperature, pressure, and experiment duration. Wettability and capillary pressure of coal matrix are two additional important parameters affecting the fraction of accessible pores [25,26]. Pores that are inaccessible to CD₄ and CO₂ have been

examined for four different bituminous coals [13]. Evident from this work is that closed porosity has a negative correlation with total porosity and SSA. But no correlation was observed between closed porosity and coal rank or maceral composition. The relationship between pore accessibility and physical properties of coal has been further investigated by studying 24 bituminous coals [14] with the observation that the fraction of inaccessible mesopores (pore size range 8–25 nm) exhibits a positive correlation with both hydrogen and vitrinite contents in vitrinite-rich coals. While the relationship between closed porosity and coal properties shows obvious region dependent. Similarly, the fraction of inaccessible pores is independent of coal rank were found. Thus, these findings of Sakurovs et al. [14] are in good agreement with those of Clarkson et al. who noted that pore accessibility is both pore size and sample dependent for shale samples [18]. Most recently observed is that the fraction of nanopores (<30 nm) accessible to heavy water (D₂O) is larger than that of CD₄ for shale [19]. Bahadur et al. suggested that there are strong correlation between mineral matter contents and the closed porosity in shale samples [20].

In this study, we refine a pore accessibility model based on the fundamental theory of SANS and test its applicability. Subsequently, two coal samples with different ranks are characterized to quantify pore accessibility and compared with this new model.

2. Fundamental theory of SANS and pore accessibility estimation

2.1. Fundamental theory

Fig. 1 shows a schematic of typical SANS experimental system [27]. The incident neutron beam of a fixed wavelength is elastically

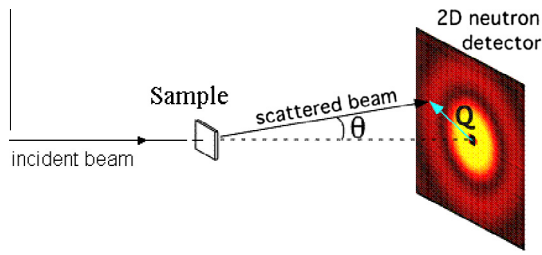


Fig. 1. The typical schematic of SANS experiment [27].

scattered by a sample with uniform thickness and illuminating volume. The angle between the scattered neutron beam and incident neutron beam is called the scattering angle, θ . Q is the magnitude of the scattering vector which has units of \AA^{-1} and can be expressed as [28]:

$$Q = \frac{4\pi}{\lambda} \sin \frac{\theta}{2} \quad (1)$$

where λ is the wavelength of the neutron beam.

The scattered neutron is detected by a two dimensional (2D) detector in an evacuated detector tube. A typical 2D plot of scattering image is illustrated in Fig. 2. For a homogenous sample with isotropic structural feature, the scattering pattern is shown as an isotropic and symmetric 2D image. In this instance, a radial averaging of the 2D image can be reduced to a one dimensional (1D) curve that can be corrected by removing the empty cell scattering, background scattering and absolute calibration [29]. Then, 1D scattering data is represented as an absolute scattering intensity $I(Q)$ versus the scattering vector Q in a log-log plot as shown in Fig. 3. The scattering intensity $I(Q)$ is defined as scattering cross section (cm^2) per scattering volume (cm^3), thus the unit of $I(Q)$ is cm^{-1} .

For microstructural analysis of porous materials, the two phase approximation has been widely applied [21]. Based on the two phase assumption, the scattering intensity $I(Q)$ can be quantified as [30]:

$$I(Q) = 4\pi(\Delta\rho^*)^2 \varnothing(1 - \varnothing) \int_0^\infty r^2 \gamma_0(r) \frac{\sin(Qr)}{Qr} dr \quad (2)$$

where $(\Delta\rho^*)^2$ is the scattering contrast between two phases. \varnothing is the volume fraction of one phase in the sample. $\gamma_0(r)$ is the correla-

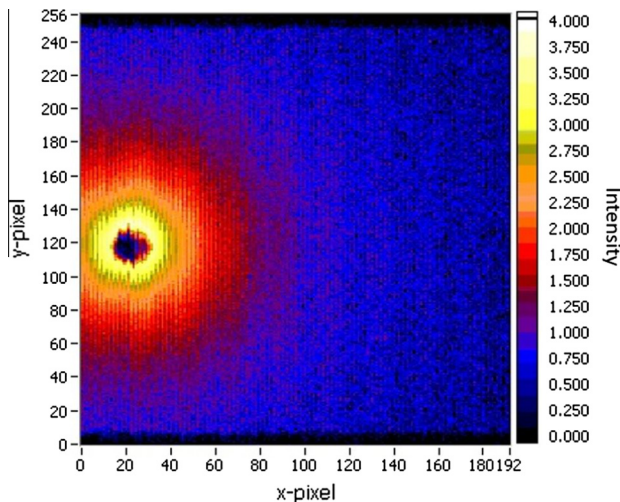


Fig. 2. The typical captured 2D neutron scattering image. The strong scattering arises due to the pores in the material. The isotropic pattern indicates that the pores are randomly aligned in the sample.

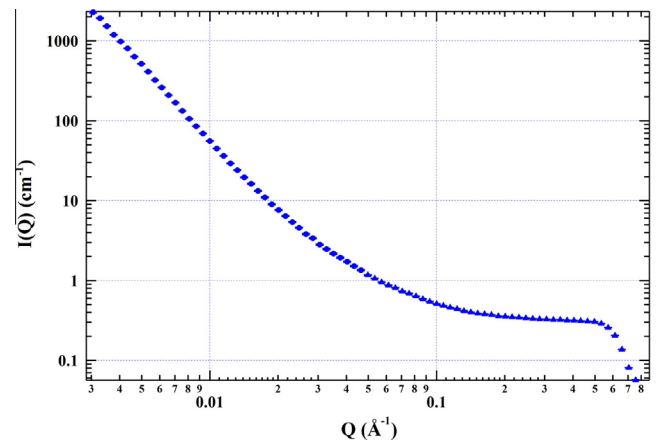


Fig. 3. The reduced 1D scattering log-log plot from 2D scattering image.

tion function and $\int_0^\infty r^2 \gamma_0(r) \frac{\sin(Qr)}{Qr} dr$ is the Fourier transform of $\gamma_0(r)$. In a two phase porous medium, these two phases are void pores and solid matrix. The scattering contrast can be expressed as:

$$(\Delta\rho^*)^2 = (\rho_s^* - \rho_f^*)^2 \quad (3)$$

where ρ_s^* and ρ_f^* are the homogenous scattering length density (SLD) of solid matrix and fluid in the void pores, respectively. The SLD of each phase can be estimated from the density and chemical composition of each phase [21] as:

$$\rho^* = \frac{N_A d}{M} \sum_j p_j \left(\sum_i s_i b_i \right)_j \quad (4)$$

where N_A is Avogadro's constant (equals to 6.022×10^{23}). d is the bulk density. M is the pseudo-molar mass of each phase. p_j is the proportion of compound j in the mixture. s_i is the proportion of nucleus i in compound j . b_i is the coherent scattering amplitude of nucleus i .

2.2. Proposed pore accessibility model

Compared to MIP and LPGA, the advantage of both small-angle X-ray scattering (SAXS) and SANS is that they can detect both open and closed pores for certain specific fluids. Moreover, highly pressurized CD_4 or CO_2 , different ratios of $\text{H}_2\text{O}/\text{D}_2\text{O}$, and cyclohexane mixture can reach the zero average contrast (ZAC) condition, which makes the SANS technique useful to investigate closed pores in rocks [31]. A new method was proposed to estimate the fraction of pores accessible to penetration by CD_4 and CO_2 [10] as:

$$\frac{I(Q, \text{ZAC})}{I(Q, \text{VAC})} \cong 1 - C_{AC}(Q) \quad (5)$$

where $I(Q, \text{ZAC})$ and $I(Q, \text{VAC})$ are scattering intensity of the ZAC and vacuum conditions, respectively. $C_{AC}(Q)$ is the fraction of accessible pores, defined as the ratio of the volume of accessible pores to the total pore volume at a given Q . It is anticipated that the estimation of the fraction of accessible pores $C_{AC}(Q)$ is constrained in a certain range of Q . The strong densification effect of CD_4 and CO_2 occurring in nanopores makes it difficult to estimate the fraction of accessible pores for small pores (high Q) [13]. Due to this limitation, we investigated and estimated the pore accessibility for a range of Q from 0.00305 to 0.0152\AA^{-1} , which corresponds to a range of pore radii between 16 and 82 nm for our coal samples.

Recently, many researchers have investigated the fraction of accessible pores for both coal [13,14,16] and shale [16,18–20] using SANS. In this study, we propose a pore accessibility model

based on the work of Melnichenko et al. [10] shown in Eq. (5). Theoretically, the fraction of accessible pores is a function of the scattering vector Q or pore size R in fractal systems such as coal. The interface between pores and the rock matrix shows both mass and surface fractals for coals [14]. Scattering of coal fractal system is represented by a power law over a wide pore size range in larger pores (low Q) [21]. The intensity of power law scattering can be expressed as [32]:

$$I(Q) = C_p Q^{-\alpha} + B \quad (6)$$

where C_p is a Q -independent constant and depends on the contrast between pores and solid matrix. α is the exponent of the power law, which describes the fractal nature of the object. B is the incoherent background. After subtraction of the incoherent background, we obtain:

$$I_{\text{subtracted}}(Q) = C_p Q^{-\alpha} \quad (7)$$

Importantly, the scattering intensity of the ZAC condition is contributed by the inaccessible pores in the two phase approximation [10]. If we assumed that both total pores detected from the vacuum condition and closed pores detected from the ZAC condition are fractal systems then background-subtracted scattering intensities of both vacuum and ZAC conditions can be represented by power law scattering as:

$$I_{\text{subtracted,VAC}}(Q) = C_{p,VAC} Q^{-\alpha_{VAC}} \quad (8)$$

$$I_{\text{subtracted,ZAC}}(Q) = C_{p,ZAC} Q^{-\alpha_{ZAC}} \quad (9)$$

Substituting Eqs. (8) and (9) into Eq. (5) yields the following result:

$$\frac{C_{p,ZAC} Q^{-\alpha_{ZAC}}}{C_{p,VAC} Q^{-\alpha_{VAC}}} \cong 1 - C_{AC}(Q) \quad (10)$$

Rearranging Eq. (10), the fraction of accessible pores is a function of the scattering vector and can be expressed as:

$$C_{AC}(Q) \cong 1 - \frac{C_{p,ZAC}}{C_{p,VAC}} \times Q^{(\alpha_{VAC} - \alpha_{ZAC})} \quad (11)$$

It is evident that if $\alpha_{VAC} = \alpha_{ZAC}$ i.e., the slope of power law scattering is same for the vacuum and ZAC conditions then the fraction of accessible pores becomes Q -independent. Thus, origin of Q -dependent accessible porosity in sample is caused by different fractal dimensions corresponding to vacuum and ZAC conditions. Hence, Q -dependent fraction of accessible pores indicates that the fractal structure of the pore-matrix for ZAC condition is different from that for vacuum condition. We define parameters a and b to simplify Eq. (11) as:

$$a = \frac{C_{p,ZAC}}{C_{p,VAC}} \quad (12)$$

$$b = \alpha_{VAC} - \alpha_{ZAC} \quad (13)$$

where a is the ratio of contrast factor between ZAC and vacuum conditions. b is the difference in the power law exponent between vacuum and ZAC conditions. Eq. (11) is reduced to:

$$C_{AC}(Q) \cong 1 - aQ^b \quad (14)$$

Eq. (14) can be used to estimate the fraction of accessible pores as a function of the scattering vector. The scattering vector Q directly correlates to the pore size and has been modeled by Radlinski et al. using numerical simulation for polydisperse porous media such as coal [33]. The correlation is given as:

$$R \cong 0.25/Q \quad (15)$$

where R is the pore radius in nanometers and Q is the scattering vector with units of \AA^{-1} . Rearranging Eq. (15) and substituting it

into Eq. (14), the pore accessibility becomes a function of pore radius as:

$$C_{AC}(R) \cong 1 - a \times (0.25)^b \times R^{-b} \quad (16)$$

We define parameters a' and b' to simplify Eq. (16) as:

$$a' = a \times (0.25)^b = \frac{C_{p,ZAC}}{C_{p,VAC}} \times (0.25)^{\alpha_{ZAC} - \alpha_{VAC}} \quad (17)$$

$$b' = -b = \alpha_{ZAC} - \alpha_{VAC} \quad (18)$$

By substituting Eqs. (17) and (18) into Eq. (16), the pore accessibility is modified into a simple power-law function as:

$$C_{AC}(R) \cong 1 - a'R^{b'} \quad (19)$$

The final power-law accessibility model of Eq. (19) can be used to estimate fraction of accessible pores as a function of pore size. The relationship will be employed to quantify the pore accessibility of coals in this study.

3. Pore characterization experiments

3.1. Sample preparation

Two coal samples were collected as bulk samples from underground at two different coal mines – one sub-bituminous coal from the northern San Juan Basin in New Mexico and the other anthracite from Hazleton in Pennsylvania. The samples were comprehensively characterized to obtain the necessary input parameters for the SANS interpretation and modeling. For the SANS experiment, based on the sample preparation guideline provided by the scientists from Oak Ridge National Laboratory (ORNL), the two coals were pulverized by hand to a particle size ~ 0.5 mm. The pulverized samples were then stored in an environmental chamber to prevent weathering and to retain moisture content constant. The samples were removed from the chamber before transport to ORNL (~ 48 h), where each sample was then loaded into the high pressure sample holder for the SANS experiment.

3.2. SANS experiment

The SANS experiments were conducted using the general-purpose small angle neutron scattering diffractometer (GP-SANS) at ORNL [34]. Powders of particle size ~ 0.5 mm optimize average scattering information for all orientations of pores in the samples, and were used here. The powder samples were loaded into aluminum cells to a thickness of ~ 1.7 mm – the thinness of the samples maximally reduces the effect of multiple scattering. Once loaded, the aluminum cells were placed into high-pressure cells with a capacity of 1000 bar (100 MPa). The neutron wavelength λ was 6 \AA and the wavelength spread $\Delta\lambda/\lambda$ was 0.13 for the experiment. Sample detector distances were chosen at 0.3 and 18.5 m, which cover an overall range of scattering vectors $0.00305 < Q < 0.5 \text{\AA}^{-1}$. And all the scattering intensities were normalized to absolute intensity by using the effective thickness of powder samples and the secondary standard [35].

Initially, the two coal samples were tested under a vacuum to quantify the vacuum background scattering intensity. For each coal sample, Argon was injected at 68 bar (6.8 MPa), 340 bar and 476 bar in a stepwise manner and the scattering intensities were measured and recorded at each pressure step. Then the Argon was bled out. After the completion of the Argon cycle, CD_4 was injected at 20 bar (2 MPa), 40 bar, 68 bar and ZAC pressure (340 bar for San Juan sample and 476 bar for Hazleton sample) for each coal sample to detect scattering intensity changes. We used CD_4 for SANS testing rather than CH_4 is because the

deuterium atom has a positive SLD rather than negative for the hydrogen atom [36], and high pressure CD₄ saturated in pores can reach the ZAC condition. In addition, using CD₄ reduces the incoherent background signal of the hydrogen atom contributing to total neutron scattering intensity [37].

4. Experimental results and discussions

4.1. Sample characterization

Table 1 shows the mineral composition and petrophysical properties of the two coal samples. X-ray diffraction (XRD) analysis (Materials Research Institute, Penn State) identifies the composition as comprising Quartz, Kaolinite, and Tobelite. Carbon, hydrogen and nitrogen contents were characterized and quantified by LECO (Energy Institute, Penn State). The Hazleton coal is a vitrinite-rich meta-anthracite with vitrinite reflectance >5%, and the San Juan coal is a vitrinite-rich sub-bituminous coal with a much higher volatile content than Hazleton anthracite. Both samples have equivalent ash content, and, as expected, the carbon content of the Hazleton anthracite is higher than that of the sub-bituminous San Juan coal. Conversely, the hydrogen and nitrogen contents for the San Juan coal are approximately double those for Hazleton coal. Effective SLD was estimated from the weighted volumetric percentage of different SLDs of the chemical components for each sample. From this, the SLD of the San Juan coal is smaller than that for the Hazleton coal, which may suggest that coal with higher hydrogen content has lower SLD due to hydrogen atom having a negative scattering length.

4.2. SANS results with CD₄ pressurization

Figs. 4 and 5 show scattering intensity $I(Q)$ as a function of scattering vector Q with different pressures of CD₄ penetration for both San Juan and Hazleton coals. In the low Q range, $I(Q)$ decreases with increasing CD₄ pressure for San Juan coal. For Hazleton coal, no obvious $I(Q)$ decrease is observed in the low Q region for the CD₄ pressure less than 40 bar, which may be attributed to the complex pore structure of high rank coals. Conceptually, the average density of the pore-filling fluid, CD₄ for this case, increases with an increase in injection pressure due to not only the compression of the gas but also the sorption of the gas on internal pore surfaces. This change in average density could lead to an increase in SLD of the pore in the low Q range, which results in a decrease of the scattering contrast between larger pores (low Q) and the solid matrix.

Interestingly, $I(Q)$ increases with increasing pressure of CD₄ in the high Q range (micro-/nano-pore range) for both coals. This suggests that the SLD contrast in the micropores increases with increasing CD₄ pressure. This may be due to the strong densification of CD₄ in micropores, which makes the SLD of CD₄ in the micropores significantly larger than the SLD of coal matrix [13]. The different scattering behaviors with various gas pressures for different ranges of Q can be explained by the different gas storage mechanisms operating in the larger pores (low Q) relative to those in the smaller pores (high Q). There are two gas storage mechanisms in dry coals, namely, compressive storage governed by the equation of state (EOS) and the absolute adsorption governed by the Gibbs thermodynamic energy balance [38–40]. These two storage mechanisms are concurrent in coal, but the dominant mechanism is both pore size and pressure dependent. For large pores, the primary storage mechanism is the storage by bulk compression since the absolute adsorption capacity is minimal and negligible compared to that stored as free gas. Whereas, the adsorptive storage becomes dominant in the micro-/nano-pores due to the high SSA and surface tension of the micro-porous matrix. The SLD of

Table 1
Characterization of two coal samples.

Sample	Quartz (%)	Kaolinite ^a (%)	Tobelite ^a (%)	Carbon ^b (%)	Hydrogen ^b (%)	Nitrogen ^b (%)	Vitrinite ^c (%)	Inertinite ^c (%)	Liptinite ^c (%)	Vitrinite reflectance ^c (%)	Ash ^d (%)	Volatile matter ^d (%)	Fixed carbon ^d (%)	Helium density (g/cm ³)	Effective SLD ^e ($\times 10^{10}$ cm ⁻²)
San Juan coal	4.71	24.56	/	63.95	5.66	1.12	76.5	9.5	14.0	0.40	12.16	42.32	45.52	1.33	3.66
Hazleton coal	/	/	8.86	88.10	2.30	0.74	95.2	3.5	1.3	5.72	10.51	3.71	85.78	1.58	3.90

^a Mineral composition were got from XRD experiment.

^b Carbon, hydrogen and nitrogen contents were got from LECO experiment.

^c Maceral composition and vitrinite reflectance were approximate values.

^d Ash, volatile matter and fixed carbon were estimated from Penn State coal bank.

^e Effective SLD were calculated by helium density and chemical composition.

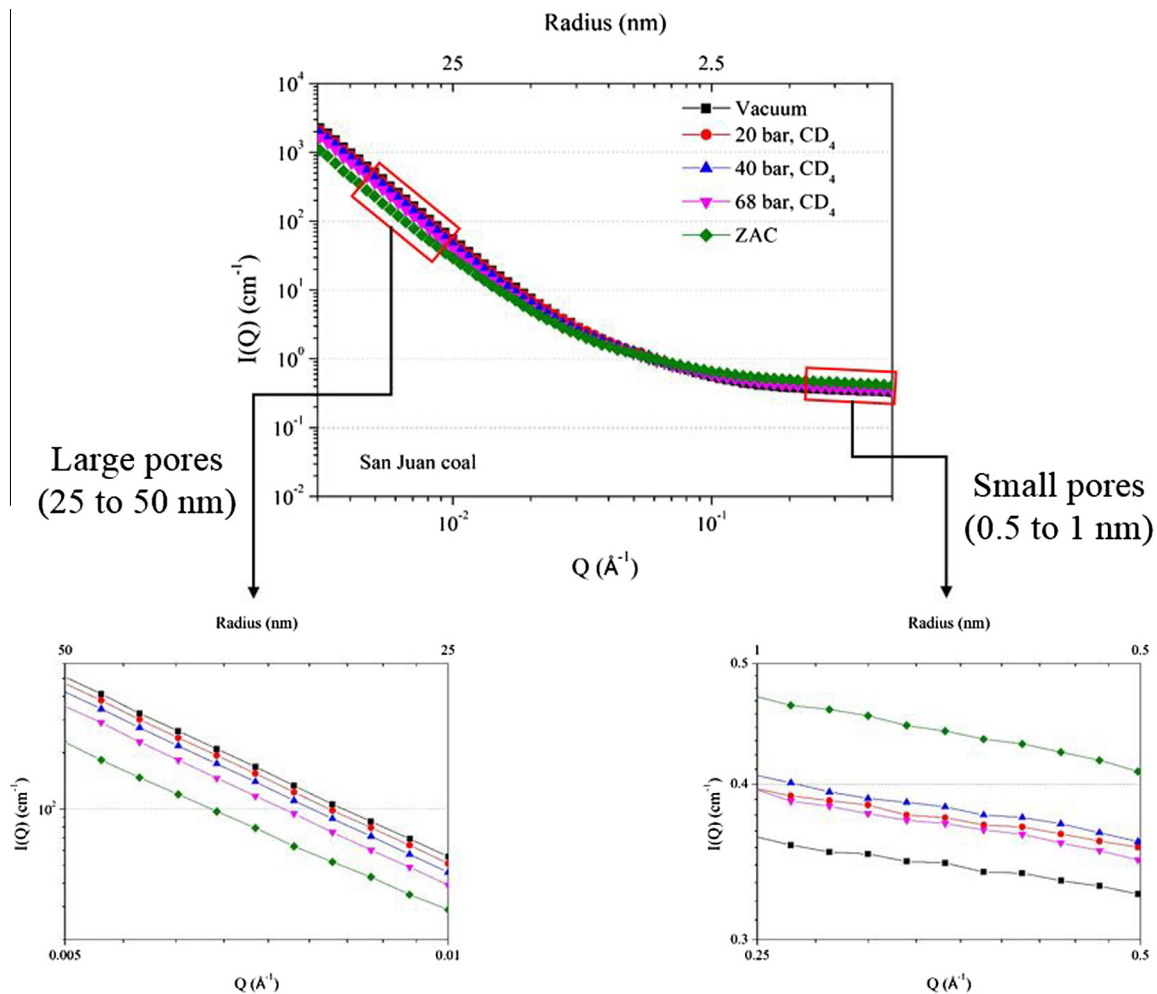


Fig. 4. Scattering intensity as function of pore size and CD_4 pressure for San Juan coal.

pressurized CD_4 can easily reach the SLD of the coal matrix in the small pores, which may suggest that different sized pores are surrounded by matrix with a different density and composition [19]. In addition, the $I(Q)$ is nearly flat in the high Q range, which may be due to the combined effects of condensation/densification of CD_4 [13], the incoherent background of the hydrogen [31], structural heterogeneity [22], and disordered adsorption of CD_4 molecules in the micropores [41]. The scattering intensity is linear in the large pore (low Q) range for both San Juan and Hazleton coals suggesting broad size distribution of the pores in these two samples [32].

Fig. 6 shows the comparison of SANS results for both San Juan and Hazleton coals under a vacuum. The SANS data in a vacuum contains information on the pore structure from both open and closed pores of the two coal samples. The $I(Q)$ of San Juan coal is higher than that of Hazleton coal in both high Q and low Q ranges. The flat scattering tail of the San Juan sample is higher than that of the Hazleton sample at high Q suggesting higher incoherent background of the San Juan coal, which may be attributed to its higher hydrogen content than the Hazleton coal [42]. In the large pore (low Q) range, a higher scattering intensity for the San Juan coal than that of Hazleton coal may be due to the larger porosity of San Juan sample [23,36]. Scattering intensity of the San Juan coal decreases smoothly with an increase in Q and reaches the flat scattering tail at a pore radius of ~ 1.25 nm. While the $I(Q)$ of the Hazleton coal also decreases smoothly, it reaches the flat scattering tail at a pore radius of ~ 6.25 nm. This may be due to San Juan coal

contains more mesopores or most of nanopores at pore sizes smaller than 6.25 nm are embedded in organic matter at which the nanopore wall has a relatively high hydrogen content, which negligibly contributes to the scattering intensity in Hazleton coal [23].

4.3. Pore accessibility estimation and modeling

As described in Eq. (7), $I_{\text{subtracted}}(Q)$ is the essential parameter for the accurate estimation of pore accessibility. During data interpretation, the incoherent background was first subtracted from the absolute $I(Q)$ under both vacuum and ZAC conditions. This subtraction may increase the errors or uncertainties of the pore accessibility and porosity results especially in the small pore range [43]. In addition to the effect of incoherent background, the mechanical compression of pores also influences the solid-pore structure during the SANS experiment, which may indirectly affect the scattering intensity. The magnitude of these effects may be determined based on poromechanical arguments [46]. As conceptually shown in Fig. 7, the mechanical compression significantly reduces the pore size due to the small bulk modulus of the coal [4,44–46]. Therefore, the scattering intensity due to mechanical compression should be corrected from the absolute intensity. Experimentally, Argon, a non-sorbing gas, was initially used to measure the background intensity due to gas pressurization alone. Finally, a correction to the scattering intensity was recovered by subtracting the effects of the incoherent background and the mechanical-compression-induced scattering intensity. Thus, the corrected

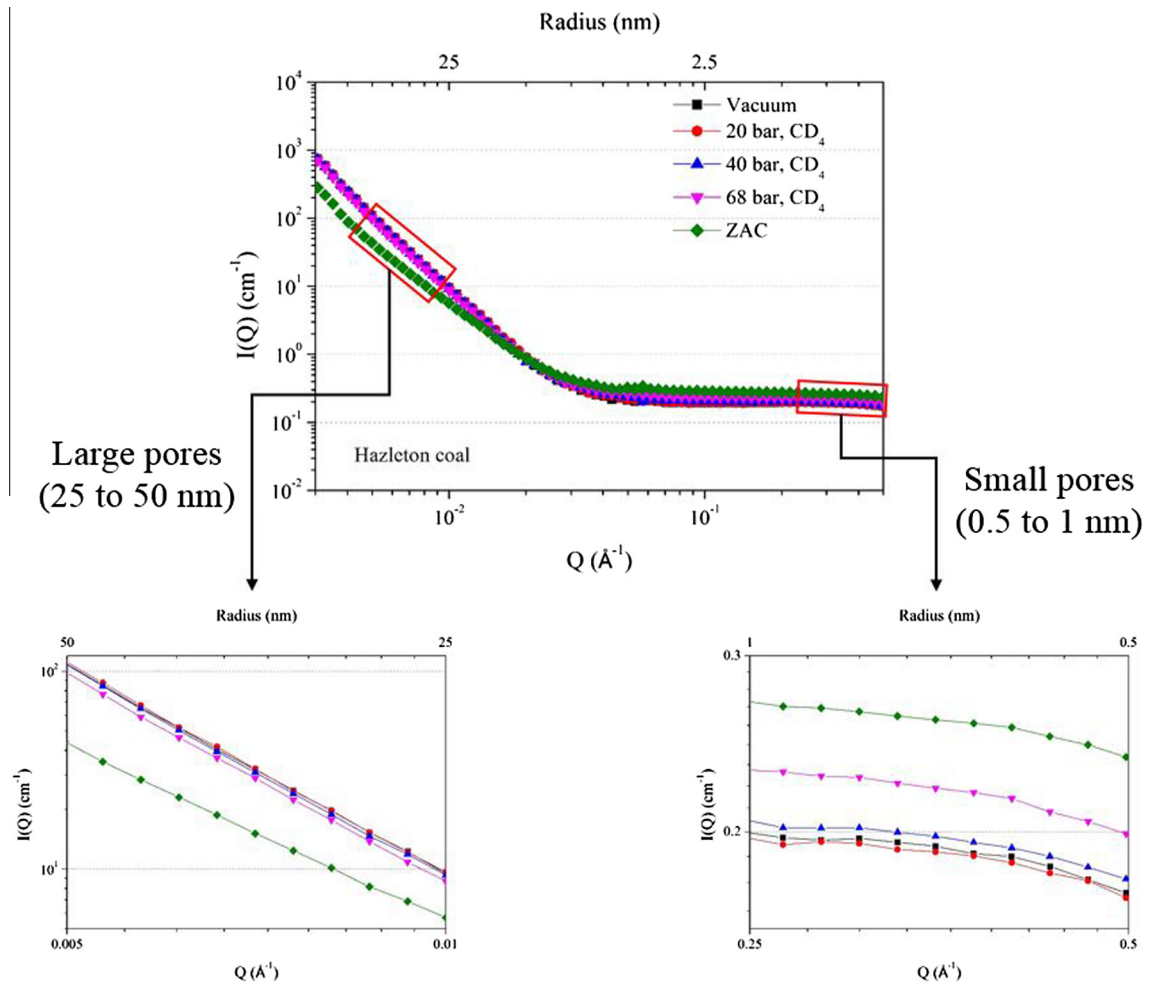


Fig. 5. Scattering intensity as function of pore size and CD₄ pressure for Hazleton coal.

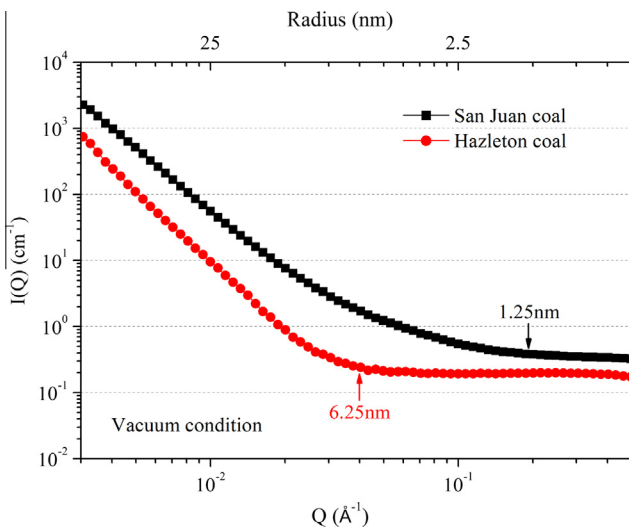


Fig. 6. Scattering intensity comparison at vacuum condition between San Juan and Hazleton coals.

scattering intensity was used to experimentally estimate the pore accessibility through Eq. (5).

Fig. 8 shows the measured pore accessibility together with the modeled results for both San Juan and Hazleton coals. Modeled

results were regressed using Eq. (19) for both samples. Parameters a' and b' in Eq. (19) were fitted to the experimental data using curve fitting (routines in Matlab), which are shown in Table 2. The fraction of accessible pores increases with an increase in pore size for both samples. This is expected since, due to their larger size, the large pores tend to be interconnected while the small pores have higher chance of being isolated. This finding also agrees with previously reported results [14], where 24 bituminous coals were used to estimate the fraction of inaccessible pores. Hazleton coal has a higher percentage of pore accessibility than the San Juan coal in the pore size range 40–82 nm. While the fraction of accessible pores of Hazleton coal is smaller than that of San Juan coal when the pore size is smaller than ~40 nm. When the pore radius is ~16 nm, the fraction of accessible pores for the San Juan coal is ~37% and it is only ~20% for Hazleton coal. This may be due to the coalification process, which changed the maceral shapes and disconnected or compressed open pores into the pores of mesopore and micropore size range. Another message from Fig. 8 is that the majority of the micro-/nano-pores are inaccessible to CD₄. The inaccessible pores do not contribute to gas transport, but may significantly influence the strength of the coal and the geomechanical response of the reservoir to primary CBM depletion as well as to CO₂-ECBM [47,48]. The inaccessible pores influence the strength of the solid skeleton, which may ultimately influence the bulk strength of coal since it is statistically determined by the micro-structural architecture [49].

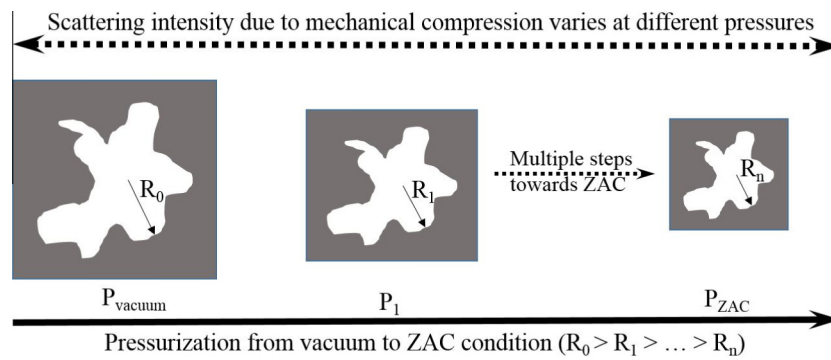


Fig. 7. Illustration of pore structure evolution during gas pressurization.

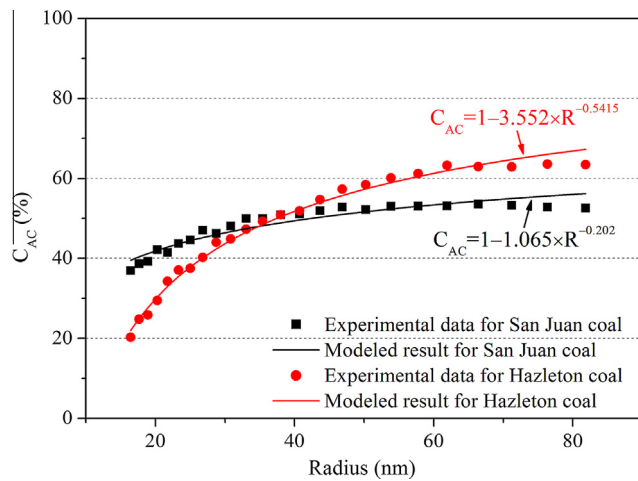


Fig. 8. Experimental and modeled pore accessibility as function of pore size for San Juan and Hazleton coals.

Fig. 9 shows rate of change in pore accessibility versus the pore radius. The slopes of the two curves in Fig. 8 give this rate of change. The derivative of pore accessibility by pore radius can be expressed as:

$$\frac{dC_{AC}(R)}{dR} \cong -a'b'R^{b'-1} \quad (20)$$

In Fig. 9, this derivative for the Hazleton coal curve is always larger than that for San Juan coal in the pore radius range 16–82 nm – the pore accessibility of the Hazleton coal increases faster than that for the San Juan coal in this pore range. When $\frac{dC_{AC}(R)}{dR}$ is less than 0.004, the pore accessibility of both coals become relatively constant, which suggests that pore accessibility is independent of pore size. It means when the pore radius is larger than ~ 27.5 nm for San Juan coal and ~ 55 nm for Hazleton coal, the pore accessibility is fairly constant for these two samples as shown in Figs. 8 and 9.

It is notable that we used powdered coal samples in the SANS experiments, which represent the average pore structures of these samples [22]. Pore accessibility estimated in Fig. 8 may be overestimated in the direction perpendicular to the coal bed and

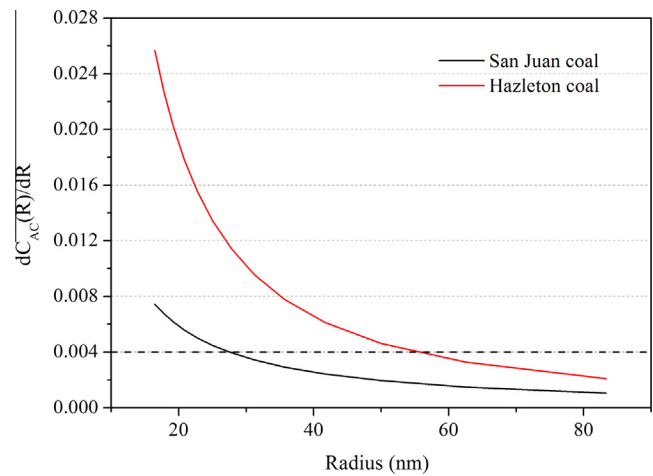


Fig. 9. Derivative of pore accessibility as function of pore size for San Juan and Hazleton coals.

underestimated in the direction parallel to coal bed for the two coal samples due to the effects of in-seam anisotropy. Effort will be made to quantify this anisotropic pore accessibility by using intact wafer samples recovered both parallel and perpendicular to bedding directions.

4.4. Application of the proposed power-law accessibility model and discussion

In order to test the applicability of the proposed power-law model in Eq. (19), another two coal samples (Coal #8 and #20) were selected from the data of Sakurovs et al. [14]. Fig. 10 shows pore accessibility with modeled results for two bituminous coals in the pore size range between 0 and 100 nm. The modeled result for coal #8 in Sakurovs et al.'s work agrees well with the experimental data. For coal #20, the model works well when the pore radius is greater than 20 nm, and it underestimates the fraction of accessible pores when the pore radius is less than 20 nm. Combining the results from Figs. 8 and 10, we may conclude that

Table 2

Fitted parameters of power-law accessibility model for two coals in this study and two coals from Sakurovs et al.'s results.

Source	Sample	a'	b'	a	b	Adjusted R ²
This study	San Juan coal	1.065	−0.202	1.41	0.202	0.892
	Hazleton coal	3.552	−0.5415	7.528	0.5415	0.9885
Sakurovs et al. [14]	Coal 8	0.8907	−0.4685	1.705	0.4685	0.8726
	Coal 20	2.667	−0.4358	4.879	0.4358	0.9391

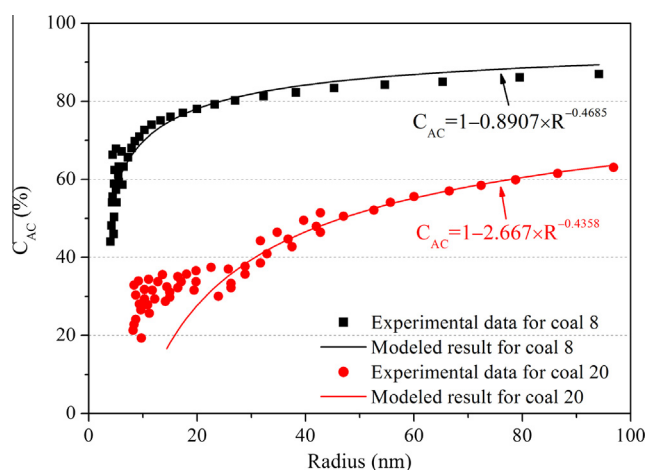


Fig. 10. Experimental and modeled pore accessibility as function of pore size for two bituminous coals (processed from Sakurovs et al.'s results).

the proposed power-law accessibility model can be successfully applied to quantify the fraction of accessible pores.

From Table 2, the parameter b' is negative for these four coals. The power law exponent describes the fractal nature of the system with the relationship $\alpha = 6 - D_s$ for a surface fractal, which may be suitable for both vacuum and ZAC conditions. The parameter b' may be equal to the difference in surface fractal dimension between vacuum and ZAC conditions ($b' = D_{s,VAC} - D_{s,ZAC}$). It is notable that the inaccessible pores occur in two forms: (1) closed or disconnected pores; (2) open pores whose size are smaller than the molecular diameter of the penetrating fluid molecule, for instance, CD_4 in this study. This finding suggests the pores inaccessible to CD_4 have a higher surface fractal dimension than that of accessible pores. The fractal dimension of porous coals is affected by various factors, including coalification, gas generation and migration, rock compaction, tectonic movement, and rock heterogeneity.

However, some of the previous SANS data in the literature (such as coal 1 [10], porous silica [10], shale MM1 sample [16] and shale 172 sample [19]) indicate that pore accessibility is independent of pore size within the range between 0 and 100 nm. It is interesting to note that the fraction of accessible pores first decreases with an increase in pore radius then increases after the pore radius is larger than ~ 40 nm for Seelyville coal [10] and Spr 879 coal [16]. Importantly, these results are unexpected since small pores tend to be isolated from each other. The higher accessibility for very small pores may be attributed to the incoherent background and/or mechanical compression effects. The accurate subtraction of the incoherent background and the precise correction for mechanical compression may influence the final accessibility results. If these two effects are trivial to the estimation of pore accessibility, then the pore accessibility for those samples in the literature will not follow the proposed power-law model. In these cases, further investigation will be needed to comprehensively describe the pore accessibility.

5. Conclusions

A theoretical model is proposed to quantify pore accessibility for methane in two coals based on the scattering intensities at both vacuum and ZAC conditions. The proposed model presents a power-law relationship between the pore accessibility and the pore size (pore radius) as given in Eq. (19). Two coal samples with different ranks were measured by SANS and the pore accessibility

were quantified for both coals. Based on both theoretical and experimental works, a few conclusions can be drawn and listed below:

- The scattering intensity should be corrected by both the incoherent background and the mechanical compression effects before it is used for the estimation of pore accessibility.
- The scattering intensity decreases with increasing CD_4 pressure in larger pores (low Q), while it increases with increasing CD_4 pressure in smaller pores (high Q) for these two coals (Figs. 4 and 5).
- The densification effect is elevated for small pores since the storage mechanism is dominated by adsorption for both coals.
- The scattering intensity of San Juan coal is larger than that of Hazleton coal in the total pore range (0.5–82 nm) at vacuum condition (Fig. 6).
- Pore accessibility of Hazleton coal is smaller than that of San Juan coal when the pore radius is smaller than 40 nm and larger than that of San Juan coal in the pore size range 40–82 nm (Fig. 8).
- The majority of the small pores are inaccessible to CD_4 . Only 20% of pores are accessible to CD_4 for Hazleton coal and 37% for San Juan coal when the pore radius is 16 nm as shown in Fig. 8.
- For these tested two samples, pore accessibility and pore radius follows a power-law relationship.

Acknowledgments

This work is a partial result of support by NSF CBET – Fluid Dynamic Program (CBET – 1438398) and by an Open Research Project through the State Key Laboratory of Coal Resources and Safe Mining from China University of Mining and Technology in Beijing (SKLCSRSM13KFA01). The research at the Oak Ridge National Laboratory High Flux Isotope Reactor was sponsored by the Laboratory Directed Research and Development Program and the Scientific User Facilities Division, Office of Basic Energy Sciences, U.S. Department of Energy. This research was supported in part by the ORNL Postdoctoral Research Associates Program, administered jointly by the ORNL and the Oak Ridge Institute for Science and Education.

References

- [1] Annual energy outlook; 2014.
- [2] Gray I. Reservoir engineering in coal seams: part 1—the physical process of gas storage and movement in coal seams. *Spe J* 1987;2:28–34.
- [3] Liu SM, Harpalani S, Pillalamary M. Laboratory measurement and modeling of coal permeability with continued methane production: part 2—modeling results. *Fuel* 2012;94:117–24.
- [4] Liu SM, Harpalani S. A new theoretical approach to model sorption-induced coal shrinkage or swelling. *AAPG Bull* 2013;97:1033–49.
- [5] Larsen JW, Hall P, Wernett PC. Pore structure of the Argonne premium coals. *Energy Fuels* 1995;9:324–30.
- [6] Everett DH. Manual of symbols and terminology for physicochemical quantities and units, appendix, definitions, terminology and symbols in colloid and surface chemistry, part 1. *Pure Appl Chem* 1972;31:579.
- [7] Gan H, Walker PL, Nandi SP. Nature of porosity in American coals. *Fuel* 1972;51:272–7.
- [8] Clarkson CR, Bustin RM. The effect of pore structure and gas pressure upon the transport properties of coal: a laboratory and modeling study. 1. isotherms and pore volume distributions. *Fuel* 1999;78:1333–44.
- [9] Gamson PD, Beamish BB, Johnson DP. Coal microstructure and micropermeability and their effects on natural-gas recovery. *Fuel* 1993;72:87–99.
- [10] Melnichenko YB, He L, Sakurovs R, Kholodenko AL, Blach T, Mastalerz M, et al. Accessibility of pores in coal to methane and carbon dioxide. *Fuel* 2012;91:200–8.
- [11] Vassilev SV, Tascon JMD. Methods for characterization of inorganic and mineral matter in coal: a critical overview. *Energy Fuels* 2003;17:271–81.
- [12] Karacan CO. Swelling-induced volumetric strains internal to a stressed coal associated with CO_2 sorption. *Int J Coal Geol* 2007;72:209–20.

- [13] He L, Melnichenko YB, Mastalerz M, Sakurovs R, Radlinski AP, Blach T. Pore accessibility by methane and carbon dioxide in coal as determined by neutron scattering. *Energy Fuels* 2012;26:1975–83.
- [14] Sakurovs R, He L, Melnichenko YB, Radlinski AP, Blach T, Lemmel H, et al. Pore size distribution and accessible pore size distribution in bituminous coals. *Int J Coal Geol* 2012;100:51–64.
- [15] Clarkson CR, Freeman M, He L, Agamalian M, Melnichenko YB, Mastalerz M, et al. Characterization of tight gas reservoir pore structure using USANS/SANS and gas adsorption analysis. *Fuel* 2012;95:371–85.
- [16] Mastalerz M, He L, Melnichenko YB, Rupp JA. Porosity of coal and shale: Insights from gas adsorption and SANS/USANS techniques. *Energy Fuels* 2012;26:5109–20.
- [17] Nguyen TX, Bhatia SK. Characterization of accessible and inaccessible pores in microporous carbons by a combination of adsorption and small angle neutron scattering. *Carbon* 2012;50:3045–54.
- [18] Clarkson CR, Solano N, Bustin RM, Bustin AMM, Chalmers GRL, He L, et al. Pore structure characterization of North American shale gas reservoirs using USANS/SANS, gas adsorption, and mercury intrusion. *Fuel* 2013;103:606–16.
- [19] Ruppert LF, Sakurovs R, Blach TP, He L, Melnichenko YB, Mildner DFR, et al. A USANS/SANS study of the accessibility of pores in the Barnett shale to methane and water. *Energy Fuels* 2013;27:772–9.
- [20] Bahadur J, Melnichenko YB, Mastalerz M, Furrmann A, Clarkson CR. Hierarchical pore morphology of cretaceous shale: a small-angle neutron scattering and ultrasmall-angle neutron scattering study. *Energy Fuels* 2014;28:6336–44.
- [21] Radlinski AP. Small-angle neutron scattering and the microstructure of rocks. *Rev Mineral Geochem* 2006;63:363–97.
- [22] Radlinski AP, Mastalerz M, Hinde AL, Hainbuchner A, Rauch H, Baron M, et al. Application of SAXS and SANS in evaluation of porosity, pore size distribution and surface area of coal. *Int J Coal Geol* 2004;59:245–71.
- [23] Tricker MJ, Grint A, Audley GJ, Church SM, Rainey VS, Wright CJ. Application of small-angle neutron-scattering (SANS) to the study of coal porosity. *Fuel* 1983;62:1092–6.
- [24] Prinz D, Pyckhout-Hintzen W, Littke R. Development of the meso – and macroporous structure of coals with rank as analysed with small angle neutron scattering and adsorption experiments. *Fuel* 2004;83:547–56.
- [25] Kaveh NS, Rudolph ESJ, van Hemert P, Rossen WR, Wolf KH. Wettability evaluation of a CO₂/water/bentheimer sandstone system: contact angle, dissolution, and bubble size. *Energy Fuels* 2014;28:4002–20.
- [26] Plug W-J, Mazumder S, Bruining J. Capillary pressure and wettability behavior of CO₂ sequestration in coal at elevated pressures. *Spe J* 2008;13:455–64.
- [27] <http://www.ncnr.nist.gov/programs/sans/>.
- [28] Glatter O, Kratky O. Small angle X-ray scattering. Academic Press; 1982.
- [29] Kline SR. Reduction and analysis of SANS and USANS data using IGOR Pro. *J Appl Crystallogr* 2006;39:895–900.
- [30] Debye P, Bueche AM. Scattering by an inhomogeneous solid. *J Appl Phys* 1949;20:518–25.
- [31] Gethner JS. The determination of the void structure of microporous coals by small-angle neutron scattering: void geometry and structure in Illinois No. 6 bituminous coal. *J Appl Phys* 1986;59:1068–85.
- [32] Bale HD, Schmidt PW. Small-angle X-ray-scattering investigation of submicroscopic porosity with fractal properties. *Phys Rev Lett* 1984;53:596–9.
- [33] Radlinski AP, Boreham CJ, Lindner P, Randl O, Wignall GD, Hinde A, et al. Small angle neutron scattering signature of oil generation in artificially and naturally matured hydrocarbon source rocks. *Org Geochem* 2000;31:1–14.
- [34] Wignall GD, Littrell KC, Heller WT, Melnichenko YB, Bailey KM, Lynn GW, et al. The 40 m general purpose small-angle neutron scattering instrument at Oak Ridge National Laboratory. *J Appl Crystallogr* 2012;45:990–8.
- [35] Wignall GD, Bates FS. Absolute calibration of small-angle neutron-scattering data. *J Appl Crystallogr* 1987;20:28–40.
- [36] Hall PJ, Brown SD, Calo JM. The pore structure of the Argonne coals as interpreted from contrast matching small angle neutron scattering. *Fuel* 2000;79:1327–32.
- [37] Mirzaei M, Hall PJ, Jirandehi HF. Study of structural change in Wyodak coal in high-pressure CO₂ by small angle neutron scattering. *J Mater Sci* 2010;45:5271–81.
- [38] Fitzgerald JE, Pan Z, Sudibandriyo M, Robinson RL, Gasem KAM, Reeves S. Adsorption of methane, nitrogen, carbon dioxide and their mixtures on wet Tiffany coal. *Fuel* 2005;84:2351–63.
- [39] Harpalani S, Prusty BK, Dutta P. Methane/CO₂ sorption modeling for coalbed methane production and CO₂ sequestration. *Energy Fuels* 2006;20:1591–9.
- [40] Pillalamarry M, Harpalani S, Liu SM. Gas diffusion behavior of coal and its impact on production from coalbed methane reservoirs. *Int J Coal Geol* 2011;86:342–8.
- [41] Laszlo K, Czakkel O, Dobos G, Lodewyckx P, Rochas C, Geissler E. Water vapour adsorption in highly porous carbons as seen by small and wide angle X-ray scattering. *Carbon* 2010;48:1038–48.
- [42] Radlinski AP, Radlinska EZ. The microstructure of pore space in coals of different rank: a small angle scattering and SEM study. In: Mastalerz M, Glikson M, Golding SD, editors. Coalbed methane: scientific, environmental and economic evaluation. The Netherlands: Dordrecht; 1999. p. 329–65.
- [43] Bahadur J, Radlinski AP, Melnichenko YB, Mastalerz M, Schimmelmann A. Small-angle and ultrasmall-angle neutron scattering (SANS/USANS) study of New Albany shale: a treatise on microporosity. *Energy Fuels* 2015;29:567–76.
- [44] Liu SM, Harpalani S. Compressibility of sorptive porous media: part 1. Background and theory. *AAPG Bull* 2014;98:1761–72.
- [45] Liu SM, Harpalani S. Compressibility of sorptive porous media: part 2. Experimental study on coal. *AAPG Bull* 2014;98:1773–88.
- [46] Liu SM, Harpalani S. Determination of the effective stress law for deformation in coalbed methane reservoirs. *Rock Mech Rock Eng* 2014;47:1809–20.
- [47] Liu SM, Harpalani S. Evaluation of in situ stress changes with gas depletion of coalbed methane reservoirs. *J Geophys Res: Solid Earth* 2014;119:6263–76.
- [48] Zhao YX, Liu SM, Elsworth D, Jiang YD, Zhu J. Pore structure characterization of coal by synchrotron small-angle X-ray scattering and transmission electron microscopy. *Energy Fuels* 2014;28:3704–11.
- [49] Zhao Y, Liu S, Zhao G-F, Elsworth D, Jiang Y, Han J. Failure mechanisms in coal: dependence on strain rate and microstructure. *J Geophys Res: Solid Earth* 2014;119:6924–35.